1-1-1997

Surface roughening during plasma enhanced chemical vapor deposition of hydrogenated amorphous silicon on crystal silicon substrates.

David M. Tanenbaum
Pomona College

Arnaldo Laracuente

Alan C. Gallagher

Surface roughening during plasma-enhanced chemical-vapor deposition of hydrogenated amorphous silicon on crystal silicon substrates

D. M. Tanenbaum,* A. L. Laracuente, and Alan Gallagher
JILA, National Institute of Standards and Technology and University of Colorado, Boulder, Colorado 80309-0440
(Received 25 October 1996; revised manuscript received 30 April 1997)

The morphology of a series of thin films of hydrogenated amorphous silicon (*a*-Si:H) grown by plasma-enhanced chemical-vapor deposition (PECVD) is studied using scanning tunneling microscopy. The substrates were atomically flat, oxide-free, single-crystal silicon. Films were grown in a PECVD chamber directly connected to a surface analysis chamber with no air exposure between growth and measurement. The homogeneous roughness of the films increases with film thickness. The quantification of this roughening is achieved by calculation of both rms roughness and lateral correlation lengths of the *a*-Si:H film surface from the height difference correlation functions of the measured topographs. Homogeneous roughening occurs over the film surface due to the collective behavior of the flux of depositing radical species and their interactions with the growth surface. [S0163-1829(97)04932-1]

I. INTRODUCTION

Thin films of hydrogenated amorphous silicon (*a*-Si:H) have a wide range of practical applications, particularly for those applications requiring very large areas and flexible substrates. They are used in the production of commercial photovoltaic modules, thin film transistors in flat panel display systems, as well as three-color detectors in imaging systems. Efforts to reduce defects and improve stability in photovoltaic applications have increased our understanding of the material itself. While *a*-Si:H films can be grown under a wide variety of conditions, the best films are typically grown in low-power rf discharges in pure silane or silane diluted with hydrogen.[1] These films do not exhibit features of columnar growth, as seen in higher-power discharge conditions or with argon dilution. Electron microscopy studies suggest that the best-quality material is homogeneous with no irregularities visible to instruments with nanometer resolution.[2–4] *In situ* ellipsometry measurements during the growth of *a*-Si:H films suggest initial nucleation is dependent upon the substrate, but is followed by homogeneous film growth beneath a lower-Si-density, H-rich surface layer.[5]

Understanding the growth kinetics of thin films has been a major effort in materials science. The development of scanning probe techniques has resulted in a renewed effort in this area over the past several years. Theoretical studies based on the models developed in the 1950s by Herring[6] and Mullins[7] have been expanded to include a variety of additional effects including shadowing and diffusion barriers.[8] Fractal scaling models have been suggested as a way to model growth surfaces with varying success, and Monte Carlo computer simulations allow a variety of model surfaces to be calculated from a set of simple growth models and parameters.[9] Unfortunately, experimental studies of even the simplest homoepitaxial growth systems reveals a complexity beyond current physical models.[10–14] Schwoebel-Ehrlich step-edge diffusion barriers can have major consequences for epitaxial growth.[15] The present case of an amorphous material is free of this type of effect, providing an opportunity to investigate the interplay of shadowing, surface diffusion, and chemical potential in film growth.

The growth chemistry of *a*-Si:H films is more complicated than simple homoepitaxy. There are a variety of radical species in the growth flux and several types of reactions are possible between the incident flux and the growth surface depending on both local (bonding configurations, etc.) and global (substrate temperature) parameters. Models of growth recognize varying sticking coefficients, extraction reactions, precursor diffusion, hydrogen diffusion and evolution, and subsurface cross linking of silicon.[16] Monte Carlo simulations of *a*-Si:H film growth have been much more simplified.[17–19]

Experimental studies of *a*-Si:H films reveal a surprisingly large variety of inhomogeneities in the amorphous network that are not fully understood and may play critical roles in limiting *a*-Si:H device performance. Small-angle x-ray scattering data report the presence of microvoids in bulk *a*-Si:H films.[20] Pockets of clustered H atoms are reported by NMR measurements.[21] These types of features make the density of *a*-Si:H $\sim 5\%$ lower than crystalline silicon (*c*-Si). Our previous scanning tunneling microscope (STM) studies of *a*-Si:H films revealed a surprisingly wide variety of topographic features, including the incorporation of nanoparticles in the films from the plasma.[21,22] In this paper we focus on the homogeneous regions of thin films of *a*-Si:H, which represent the vast majority of the film volume. These measurements should correlate with techniques that average over large regions of the film surface.

II. EXPERIMENT

Details of the experimental apparatus have been described in previous publications.[23] It consists of an ultrahigh vacuum (UHV) analysis chamber directly connected to a small plasma-enhanced chemical-vapor deposition (PECVD) chamber by a gate valve. The analysis chamber houses a STM, a low-energy electron diffraction and Auger spectrometer system, and a variety of tools for preparation and storage of samples and STM probes. The PECVD electrode spacing

is 1.9 cm. The temperature of the chamber walls and the grounded electrode (and substrates) is maintained at ~250 °C during all film depositions. The source gas is pure silane with a pressure of ~72 Pa (540 mTorr) and the discharge depleted ~5% of the silane flow. The film deposition rate was 0.1–0.2 nm/s for all films in this study.

STM probes were etched W or PtIr wire, which was heated in vacuum prior to tunneling on *c*-Si surfaces. Tunneling on Si(100) allowed for the construction of sharp nanocolumns on the end of the probe, enabling the probe to tunnel down into the surface valleys on the *a*-Si:H.[24] Nanocolumn probes had a radius of curvature less than 2 nm with a taper of 45°–70° over the final 5 nm. This characterization was critical as all STM topographic measurements are nonlinear contact transforms of the probe and sample surfaces separated by an ~0.5 nm tunneling gap. Tunneling currents were 20–60 pA with a negative sample bias voltage (3–6 V magnitude) relative to the probe. The low-current, high-bias conditions are a result of the very low conductivity of intrinsic *a*-Si:H. A measured exponential decay in the tunneling current with increasing probe-sample separation confirms we are tunneling above the films. All STM topographic data have been analyzed after subtraction of a plane corresponding to sample tilt and removal of a small background curvature due to nonlinear thermal drift and piezoelectric creep.[25]

The substrates for the *a*-Si:H films were Si(100) wafers that were heated in UHV to ~1050 °C to remove oxide and contaminants, resulting in a 2×1 dimer reconstruction imaged by the STM. Each substrate was examined by the STM prior to film growth. Typical 100-nm^2 regions were observed to have a rms roughness σ of 0.05 nm. The substrates were transferred in vacuum to and from the deposition chamber where they were coated with *a*-Si:H film. This eliminates exposure to any contamination sources beyond those present during the growth itself.

III. DATA COLLECTION

In order to survey the *a*-Si:H film topography we looked at several different macroscopic areas on the film surface. Typically for samples described in this study six different macroscopic regions ($\approx1\ \mu$m^2, spaced more than 1 mm apart) were studied for each sample. There was no significant difference between the regions for the thin films. Inside each of these regions, a minimum of five images (100×100 nm^2) were recorded. The images have data recorded at 1-nm intervals. Images were also taken at higher resolution (0.1-nm intervals) to look for atomic scale features. All STM images are taken in constant current mode with feedback on. Some images contain distinct features believed to be nanoparticles in addition to the homogeneous roughness described below. These images are excluded from the analysis in this paper, but are the subject of a previous publication.[21]

The undoped *a*-Si:H typically has a low-field resistivity $\rho>10^9\ \Omega$ cm. A calculation of spreading resistance for current injected from a subnanometer point contact using this number suggests that it would be impossible to conduct these tunneling currents through the films. The spreading-resistance picture is incorrect here because the tunneling occurs for energies far from the conduction-band edge and the very thin *a*-Si:H films (~10 nm) are significantly doped by the heavily doped *c*-Si substrates. The band gap of *a*-Si:H is ~1.7 eV, while we applied a $V\sim5$ V between the probe and the substrate. In order to estimate the relative fraction of the voltage drop in the film and the tunneling gap, we consider the limit where no current is flowing. The tip is modeled by a small metal sphere with $r\approx1$ nm and the tunneling gap by a vacuum shell ~1 nm thick surrounded by a 100-nm-thick shell of *a*-Si:H ($\varepsilon=10\varepsilon_0$), capped by a grounded conductor. The resulting voltage drop across the film is ~10% of the voltage on the probe. A voltage drop greater than 0.5 V across the film can support a space-charge-limited current in the film of almost 100 nA if the *a*-Si:H has no deep traps.[26] The overall picture is more complicated, but electrons are tunneling into the film several eV above the Fermi level and these electrons are still in a very high field when they enter the film. The high-energy electrons travel ballistically upon entering the film and, assuming cooling rates approximately equal to 1 eV/ps,[27] traverse tens of nanometers before they thermalize. The overall transit time for the carriers is 1000 times shorter than the deep trapping time in the film.

To ensure that our images represent the true film topography, it is important to establish that we are tunneling above the surface with a relatively constant tunneling gap. In one case we evaporated a 4-nm-thick gold film over a thick *a*-Si:H film and a crystal silicon sample, effectively eliminating the voltage drop in the samples. The overall character of the images was unchanged, confirming that the features observed in the topographs of the *a*-Si:H are not dominated by electronic features.

It is simplest to consider the entire surface as a function $h(x,y)$, which defines the height at all points on a square grid. The height-difference correlation function is $G(\rho)\equiv\langle[h(x,y)-h(x',y')]^2\rangle_{x,y}$, where (x',y') represents all points a distance ρ from (x,y), the angular brackets indicate an average over the entire xy plane, and $\bar{h}$ is the mean height. As ρ becomes large, the h values become uncorrelated and $G(\rho)$ approaches $2\sigma^2$, where σ is the rms roughness. The ρ for which $G(\xi)=\sigma^2$ defines ξ, the lateral correlation length of the surface. Another reasonable choice for ξ would be the exponential rise distance of G. We have chosen the half height, as it is less influenced by oscillations in G, which are not our main focus. $G(\rho,t)$ can be easily compared with dynamic scaling models, where t represents the film thickness. The calculation of G from the data is simplified slightly from the exact expressions. We consider separations only parallel to the scan direction on the amorphous material, which has no preferred orientations. Even if there were some coupling of the underlying crystal lattice or an oriented step pattern, these would contribute to height variations about an order of magnitude smaller than those in our data.

IV. TOPOGRAPHS

Typical data recorded for the different films are shown in Fig. 1. All the images are 100×100 nm^2 with the vertical scale expanded three times the horizontal scales. Higher-

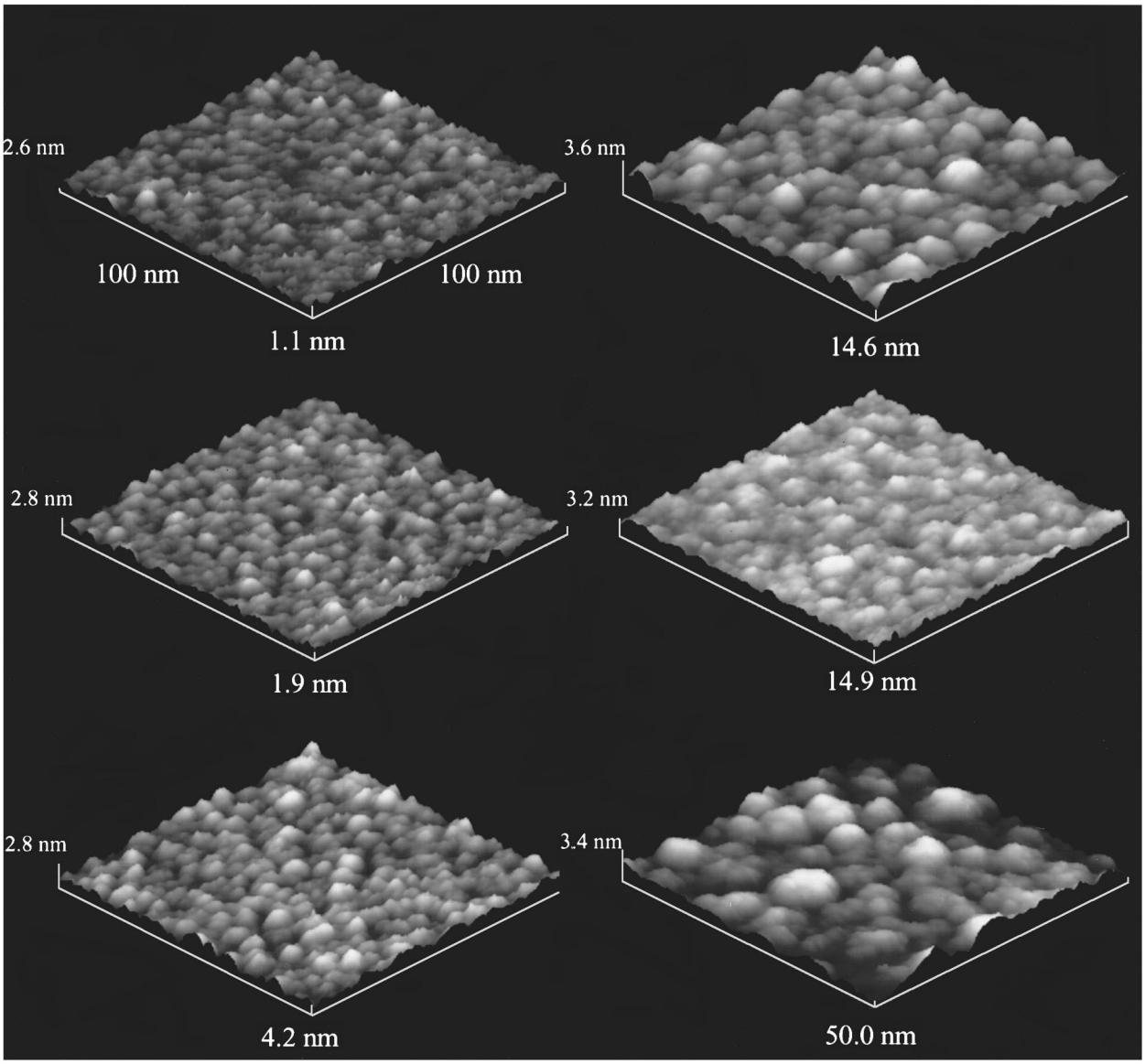

FIG. 1. Series of typical homogeneous 100-nm^2 images of the a-Si:H film surface. The total film thickness is labeled below each image. The vertical scale is expanded three times.

resolution images such as the image in Fig. 2 do not reveal individual atom sites or substantially different topographic information. Two trends should be apparent by looking at the topographs in Fig. 1. The first is uniformly lumpy surfaces, with lumps whose lateral size (ξ) grows with increasing film thickness. The second trend is a slight increase in the surface height (peak to valley, which is tied to σ) with increasing film thickness.

The height difference correlation functions $G(\rho)$ for typical surfaces of a given film thickness are plotted in Fig. 3. All the curves exhibit similar behavior for small values of ρ, sharply rising initially and eventually attaining a plateau (with oscillations in some cases) for large values of ρ. The values of σ and ξ are calculated for each individual image to estimate the uncertainties in these values. The $G(\rho)$ curves for several different images of a given thickness and their average are shown in Fig. 4.

Figure 5 displays σ and ξ as functions of film thickness t. Error bars represent one standard deviation of the values from the individual images for a given film thickness. The data are plotted on a log-log scale, as would be suggested by the dynamic scaling model described below. The lines on the plots represent the best fit of the data to a power law, although the χ^2 of these fits suggest they are not ideal for describing our data. The most obvious deviation from these trends occur for the 14.9-nm film. We expect this is the result of probe-sample contact during initial tunneling on this film, which reduced the probe sharpness, resulting in lower image resolution.

Ultimately, the topographs are still influenced by probe size. Figure 6 shows the local surface gradient in a typical image. Angles above 20° from the plane are not uncommon and valleys with such high angles are very likely to result in a change of tunneling points along the probe. Having characterized our probes, we can expect that for images where $\xi \sim 2$ nm the measured σ may be lower than the true σ and the measured ξ may be larger than the true ξ due to the probe's final radius of curvature.

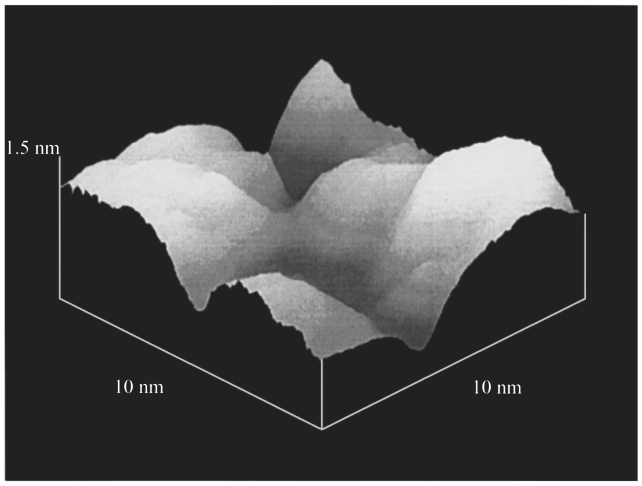

FIG. 2. High-resolution image of a 4.2-nm-thick *a*-Si:H film. The data points are collected on 0.1-nm intervals. The vertical scale is expanded three times.

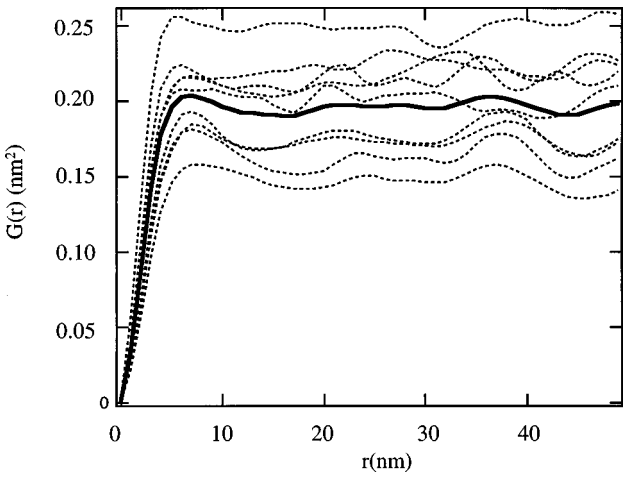

FIG. 4. Nine different measurements of the height difference correlation function $G(r)$ for different regions of a 1.9-nm-thick *a*-Si:H film and their average (solid line).

V. DISCUSSION

A. Growth models

The *a*-Si:H surface topology provides an opportunity to test different growth issues than those that dominate epitaxial growth. The surface slopes are much larger in the present case, typically 20° compared to 1° for epitaxial surfaces, and the *a*-Si:H film precursors arrive in a cosine distribution. The surface roughness observed here greatly exceeds what would be expected from statistical fluctuations in an incident precursor flux with unity film incorporation (random site growth) so that roughening due to shadowing must be very significant. Surface diffusion and enhanced incorporation probability in valleys are essential to the absence of runaway shadowing and the attainment of a compact film. The enhanced valley incorporation probability is physically expected and is normally described with a chemical potential proportional to $\nabla^2 h$. Due to the high surface angles, shadowing effects can be approximated as a term proportional to $(\nabla h)^2$, whereas diffusion and enhanced valley incorporation of a diffusing radical are proportional to $\nabla(\nabla^2 h)$ and similar

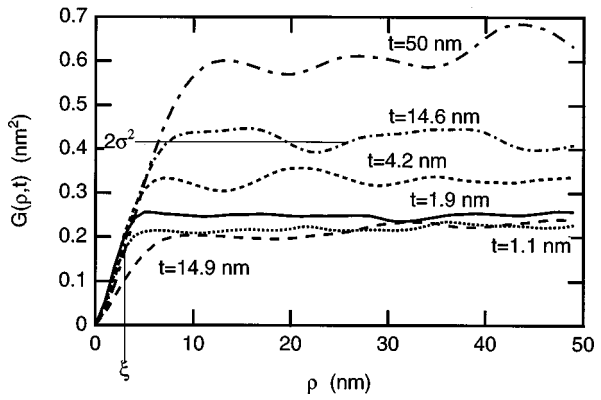

FIG. 3. Measured behavior of the height difference correlation function $G(\rho,t)$. Two times the square of the rms roughness $2\sigma^2$ and the lateral correlation length ξ are indicated for the 14.6-nm-thick film.

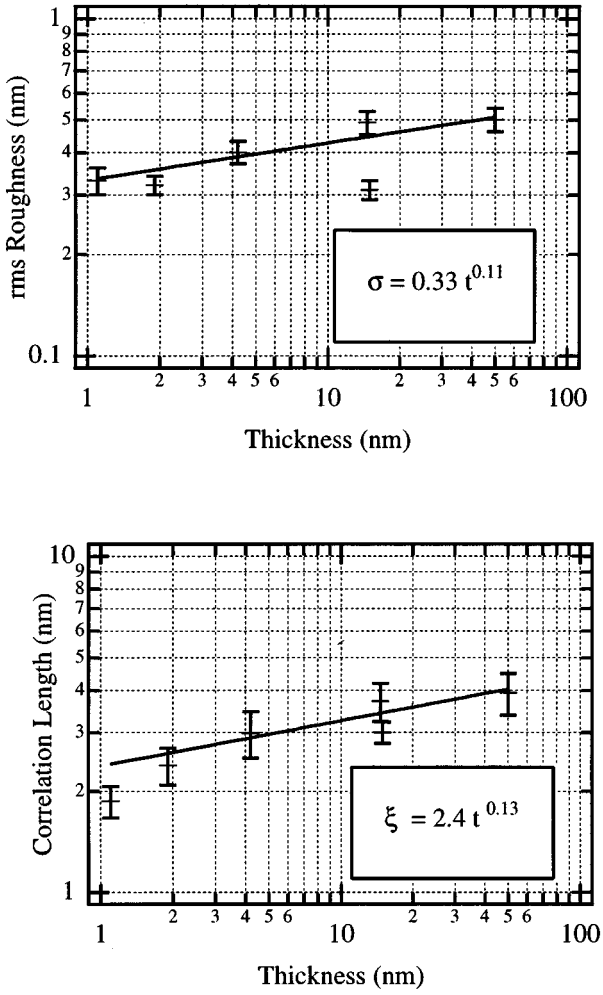

FIG. 5. The rms roughness and the lateral correlation length extracted from the $G(\rho,t)$ curves of the *a*-Si:H films. The 14.9-nm-thick film data deviate from the trends of the other films. We expect this is the result of probe sample contact during initial tunneling on this film, which reduced the probe sharpness, resulting in lower image resolution.

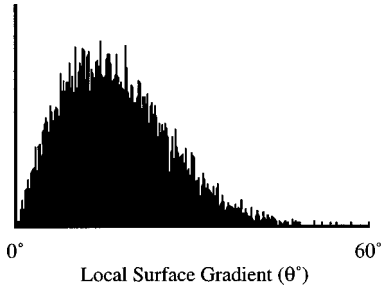

FIG. 6. Distribution of the angle of the local surface gradients of a film surface on a typical 4.2-nm-thick a-Si:H film.

terms that are always linear in h. The existence of surface roughness larger than the random site growth model would generate requires that shadowing be significant since diffusion and the chemical potential smooth the surface relative to the random site growth model. However, if shadowing is a significant term and quadratic in h, while the smoothing due to diffusion and the chemical potential are linear in h, then the shadowing will cause runaway roughness, which is not observed. The answer to this dilemma is contained in the existing chemical model for the growth of compact a-Si:H films; it is a two-step process. First, a dangling bond must be formed at the surface and then a SiH_3 molecule incorporates at the dangling bond. This provides for diffusion and a chemical potential that acts once on the dangling bonds and again on the SiH_3 molecules. The result is a smoothing that is quadratic in h. Although the importance of this two-step growth has been recognized qualitatively for some time,[16,28] we are not aware of any quantitative modeling that incorporates this phenomenon.

There have been a few Monte Carlo simulations of the growth of a-Si:H films.[17–19] The model of McCaughey and Kushner was tuned to produce as accurately as possible a fit to the behavior of a-Si:H film growth under a wide variety of conditions as this behavior was understood in the late 1980s. In comparing our data with the existing calculations, it is clear that we observe substantially lower values for σ, despite the model's bias towards valley filling. There is no reported data for the behavior of ξ in these models. A variety of changes could be added to produce an updated model.

B. Dynamic scaling hypothesis

In an effort to understand the roughening of surfaces from a more general theoretical viewpoint, Family and Vicsek have introduced the concept of dynamic scaling of surfaces.[29] There have been a variety of experimental thin-film growth systems for which this type of model appears reasonable.[30] The dynamic scaling model proposes that G can be written as $[G(\rho,t)]^{1/2} \approx \rho^{\alpha} f(t/\rho^{\alpha/\beta})$, where $f(t/\rho^{\alpha/\beta}) \approx t^{\beta}/\rho^{\alpha}$ when the argument of f is much less than 1 and where $f \approx$ const when the argument is much greater than 1. Figure 7 shows a plot of the behavior of G as predicted by this dynamic scaling theory. The qualitative behavior of Fig. 7 bears a striking resemblance to our measured $G(\rho,t)$ in Fig. 3. The critical exponents of the model, α and β, can be extracted from the experimental results revealing $\alpha = 0.8$ and $\beta = 0.1$. This fit provides a reasonable description of our film surface topology. The oscillations in the G functions sug-

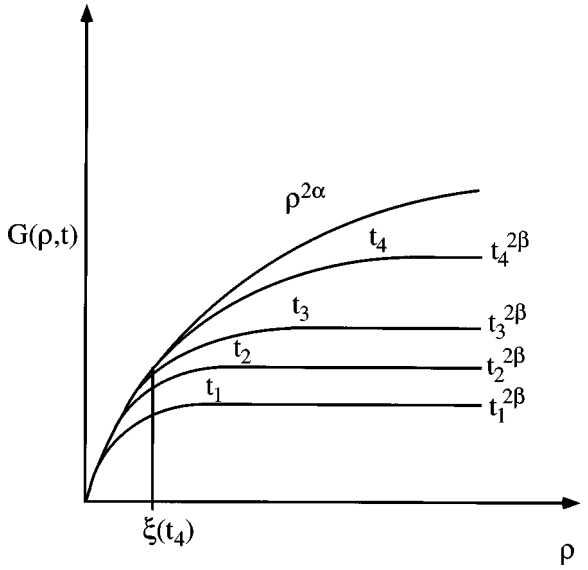

FIG. 7. Dynamic scaling model for the behavior of $G(r,t)$. The curves all collapse to the same envelope function ($r^{2\alpha}$) for small r and stabilize at a level determined by the film thickness t for large values of r.

gests that the surfaces are not actually self-affine, similar to several recent papers on homoepitaxy.[10–12]

These particular values of α and β do not appear as values described by any of the classes of continuum growth models.[9,13,31,32] The premise that a given class of processes will generate particular universal exponents in three dimensions appears to contradict some Monte Carlo studies.[33] The value of β (<0.5) agrees with the concept of mass transport moving adsorbed species from the peaks towards the valleys of the surface.

The measurement of the critical exponents does not teach us about the processes of the a-Si:H film nucleation and growth. Many of the continuum models have attempted to describe physical phenomenon relevant to film growth. Herring proposed that the chemical potential for an atom on a homogeneous surface is proportional to the curvature of the surface.[6] In a-Si:H a dangling bond on a local peak is less able to share a H atom with a nearest neighbor than a dangling bond in a local minimum due to the larger separation of such neighbors. Mullins applied Herring's chemical potential to calculate a surface evolution having the form $\partial h/\partial t \propto \nabla^4 h(x,y)$.[7] This is the dominant smoothing term introduced in continuum models in use today.[13] Bales *et al.* have attempted to formulate a description of nonlocal shadowing into these continuum models.[8]

C. Ellipsometry measurements of a-Si:H

One of the most heavily utilized techniques for learning about surface roughness of a-Si:H films has been ellipsometry, which can be performed *in situ* during film growth. Drévillon and co-workers[34,35] and Collins and co-workers[5,34–38] have examined a-Si:H grown on a variety of substrates.[5,36–40] We compare our results with those for the silicon substrates with the native oxide, which should most closely resemble our surface. To validate the complex modeling of the spectroscopy data, Lu *et al.* have performed

ambient atomic force microscope (AFM) measurements on samples of *a*-Si:H films studied by ellipsometry.[39,40] They report a linear relationship $d_s = 1.4 d_{\mathrm{rms}}(\mathrm{AFM}) + 0.4$ nm between the two methods of measuring the roughness.

According to Drévillon and co-workers, the nucleation sites have a spacing of 6.0 nm. The first 3.5 nm of film growth are represented by island growth, after which coalescence occurs. By this time a rms roughness of 1.0–1.5 nm has grown into the film topology, and this surface roughness is essentially unchanged as the film continues to grow thicker. Our data suggest a much smaller initial roughness, but the qualitative feature of a very slow increase in roughness with thickness is similar.

The work of Collins and co-workers suggests nucleation sites represented by islands separated by 3.9 nm on native oxide and the coalescence is seen to occur after the first 1.5–2.0 nm of film growth.[5,40] The growth of the surface and bulk layers of the film was extracted from the ellipsometry measurements. The data show the surface roughness increases substantially during the first 2 nm of film growth and then decays to a constant value as the bulk film grows linearly underneath it. In comparison to our data, there is a small discrepancy during the very early stages of film growth, where we see negligible decay of the surface roughness following an island coalescence. The AFM measurements reported by Lu *et al.* do not explore the initial coalescence on the growth surface.[40] The diffusion of the SiH_3 precursor may be substantially inhibited on the native silicon oxide in contrast to the *a*-Si:H film. A difference in film precursor mobility or initial nucleation may explain the discrepancy in the early stages of the two experiments. As for the longer-term behavior of the surface, ellipsometry measures only a smoothing of σ to a steady-state value after the initial nucleation, compared with our slight increase in σ with film thickness. The initial value of ξ (1.8 nm) in our data is comparable with the initial nucleation radii inferred by ellipsometry (~ 2 nm). Ellipsometry makes no evaluation of the development of the lateral correlation length with thickness.

D. Other scanning probe measurements of *a*-Si:H

There are few measurements of the as-grown *a*-Si:H film surface for thin films. Kazmerski reported STM measurements for as-grown surfaces of doped films between 0.2 and 1.0 μm thickness, noting that thinner and thicker layers had ''unacceptably rough surfaces.'' [41] Wiesendanger *et al.* examined 0.5-μm-thick films after ''gentle Ar^+-ion bombardment.'' [42] Jahanmir *et al.* and Hartmann *et al.* have published reports of STM induced modifications to *a*-Si:H films of 20- and 60-nm-thick films, respectively, in air and high-vacuum systems.[43,44]

Boland and Parsons have used a STM to study effects of hydrogen plasma etching of weak bonds in *a*-Si:H films, imaged in vacuum after dipping in dilute HF following exposure to the ambient atmosphere.[45] A phosphorus-doped 70-nm-thick film grown with 5:1 H_2 dilution on a metal substrate had a $\sigma = 0.51$ nm. The homogeneous features are less than 25 nm in lateral dimension, in agreement with the films grown in our experiment.

There are two reports of UHV STM studies of thin *a*-Si:H film surfaces that have not been deposited on crystal silicon, but rather on a different atomically flat single-crystal substrate. In a previous publication we noted exceptionally smooth films ($\sigma < 0.1$ nm) grown on GaAs.[23,46] Matsuda and co-workers published reports in which they studied the initial growth and nucleation of *a*-Si:H on highly oriented pyrolytic graphite (HOPG) substrates.[46,47] The island coalescence appears to be much slower on HOPG than we observe on *c*-Si. An interesting comparison can be made with a study of thin (less than 5 nm thick) *a*-C:H grown on both HOPG and silicon substrates by Vandentop *et al.* where a similar difference in nucleation site density and film growth was observed.[48] Typically, the critical intrinsic layer of *a*-Si:H devices is grown directly on a doped layer of *a*-Si:H film, which in turn is grown on an oxide substrate, usually SiO_x, ZnO_2, or ITO.

A very different picture of the early stages of *a*-Si:H film growth has been proposed by Deki *et al.*, based on AFM measurements in air.[49] Substrates included H-terminated *c*-Si(111). A series of films grown between 1 and 5 nm thick are all reported to have terraces similar to the substrate.[49] From this a layer-by-layer growth mode was suggested. The striking difference between these AFM measurements and our data may be the result of H_2 dilution substantially smoothing the surface via etching of the weak Si bonds or an artifact of the larger AFM probe that is in contact with the surface.

E. Diffusion length

One would like to have diffusion lengths and chemical potentials for both the dangling bonds and the SiH_3 molecules along the film surface. The importance of the substrate temperature in growth of device quality *a*-Si:H films may be balancing the increasing diffusion of SiH_3, which improves film flatness, and the loss of hydrogen from the films, which introduces more dangling bonds, degrading film flatness.[50] Collins and Yang have shown that smoothing of well-characterized polycrystalline substrate roughness by subsequent *a*-Si:H deposition determines a diffusion length between 6 and 10 nm.[38] It is not clear if this value represents mobility of the SiH_3 precursor or the dangling bond.

Our STM data characterize the growth of the film surface, including the evolution of the lateral correlation length, which cannot be seen from the ellipsometry data. An approximation of the diffusion length could be the lateral correlation length. This implies a film-thickness-dependent diffusion length, which is not expected physically. In an AFM study of growth of CuCl on CaF_2 surfaces, Tong *et al.* assumed that for length scales shorter than the diffusion length, the diffusion term presented by Mullins completely overwhelms all other effects.[51] They report values for two film thicknesses resulting in different values for the diffusion length on the initial substrate and the growing film. If the growth system resembles the general characteristics of dynamic scaling, then an increasing diffusion length as a function of film thickness will result. The diffusion length should be dependent upon the local potential energy of the substrate and the adsorbate, not overall film thickness. The lateral correlation lengths are a function of diffusion length, but a more complete model that involves diffusing dangling bonds and a variety of film precursors is needed to establish the functional relationship.

Doughty *et al.*[16] suggested that the surface reaction probability of SiH_3 on the *a*-Si:H surface is essentially independent of temperature between 20 °C and 250 °C and postulated that the reaction probability is the product of two independent terms. The first term describes the initial probability to adsorb at the point of contact and the second term is the probability to react, at any point on the surface during diffusion, before desorbing from the surface. The first term may be independent of temperature and dominated by steric factors, while the second term, normally expected to have a temperature dependence related to the relative energies of diffusion and desorption barriers, may in fact be unity under the conditions tested. In this case, SiH_3 always diffuses a sufficient distance to find a dangling bond or abstract a H atom from the surface before it has a chance to thermally desorb. Then any measured diffusion length is dominated by the average separation of the dangling bonds and not the SiH_3 precursor.

VI. CONCLUSION

We have studied the development of the growth surface of device quality *a*-Si:H films. Most of the surface area is homogeneous hilly regions with distributions of hill heights and widths that grow with film thickness. This homogeneous film growth has been characterized by the evolution of the rms roughness and the lateral correlation length as functions of film thickness. On *c*-Si substrates the initial roughness develops during the first few monolayers of film deposition, followed by a gradual increase with film thickness. The lateral correlation lengths show a slightly faster growth with increasing film thickness. There is no indication of an enhanced roughness during the initial nucleation phase on H-terminated *c*-Si substrates, as has been reported for both STM measurements of *a*-Si:H films nucleating on HOPG and ellipsometry measurements of *a*-Si:H films nucleating on *c*-Si surfaces with native oxides. Otherwise, the magnitude of the rms roughness is in reasonable agreement with the ellipsometry measurements.

A comparison of the surface rms roughness and lateral correlation length with the dynamic scaling hypothesis gives reasonable agreement, although the surfaces are not completely self-affine. The calculated dynamic scaling exponents do not match any of the current continuum growth models, but the dramatically sublinear growth of the roughness with thickness is clearly indicative of a surface smoothing mechanism, such as a chemical-potential-driven precursor diffusion to valleys, which is expected to play a key role in preventing void formation and defects in the films. The valleys in the homogeneous regions of the *a*-Si:H films appear smooth with slopes typically less than 30° from the plane and thus are not likely to be incipient voids in the material. The attainment of a compact film despite the presence of significant shadowing supports the existence of a two-step incorporation model in the PECVD growth of *a*-Si:H.

ACKNOWLEDGMENT

This work was supported by the National Renewable Energy Laboratory, under Contract No. DAD-4-1408401.

*Present address: School of Applied and Engineering Physics, Cornell University, Ithaca, NY 14853.

[1] R. A. Street, *Hydrogenated Amophous Silicon* (Cambridge University Press, Cambridge, 1991).
[2] C.-C. Tsai, J. C. Knights, G. Chang, and B. Wacker, J. Appl. Phys. **59**, 2998 (1986).
[3] J. C. Knights and R. A. Lujan, Appl. Phys. Lett. **35**, 244 (1979).
[4] J. C. Knights, in *Plasma Synthesis and Etching of Electronic Materials*, edited by R. P. H. Chang and B. Abeles, MRS Symposia Proceedings No. 38 (Materials Research Society, Pittsburgh, 1985) p. 371.
[5] Y. M. Li, I. An, H. V. Nguyen, C. R. Wronski, and R. W. Collins, Phys. Rev. Lett. **69**, 2814 (1992).
[6] C. Herring, in *The Physics of Powder Metallurgy*, edited by W. E. Kingston (McGraw-Hill, New York, 1951).
[7] W. W. Mullins, J. Appl. Phys. **28**, 333 (1957).
[8] G. S. Bales, R. Bruinsma, E. A. Eklund, R. P. U. Karunasiri, J. Rudnick, and A. Zangwill, Science **249**, 264 (1990).
[9] F. Family, Physica A **168**, 561 (1990).
[10] J. E. Van Nostrand, S. J. Chey, M.-A. Hasan, D. G. Cahill, and J. E. Greene, Phys. Rev. Lett. **74**, 1127 (1995).
[11] J. A. Stroscio, D. T. Pierce, M. Stiles, and A. Zangwill, Phys. Rev. Lett. **75**, 4246 (1995).
[12] M. D. Johnson, C. Orme, A. W. Hunt, D. Graff, J. Sudijono, L. M. Sander, and B. G. Orr, Phys. Rev. Lett. **72**, 116 (1994).
[13] J. Lapujolade, Surf. Sci. Rep. **20**, 191 (1994).
[14] J. Villain, J. Phys. (France) I **1**, 19 (1991).
[15] J. Villain, J. Phys. (France) I **4**, 949 (1994).
[16] D. A. Doughty, J. R. Doyle, G. H. Lin, and A. Gallgher, J. Appl. Phys. **67**, 6220 (1990).
[17] M. J. McCaughey and M. J. Kushner, J. Appl. Phys. **65**, 186 (1989).
[18] T. Shirafuji, S. Nakajima, Y. F. Wang, T. Genji, and K. Tachibana, Jpn. J. Appl. Phys. 1 **32**, 1546 (1993).
[19] T. Shirafuji, W. Chen, M. Yamamuka, and K. Tachibana, Jpn. J. Appl. Phys. 1 **32**, 4946 (1993).
[20] J. Shinar, H. Jia, R. Shinar, Y. Chen, and D. L. Williamson, Phys. Rev. B **50**, 7358 (1994).
[21] D. M. Tanenbaum, A. L. Laracuente, and A. Gallagher, Appl. Phys. Lett. **68**, 1705 (1996).
[22] D. M. Tanenbaum, A. Laracuente, and A. C. Gallagher, in *Amorphous Silicon Technology—1994*, edited by E. A. Schiff *et al.*, MRS Symposia Proceedings No. 336 (Materials Research Society, Pittsburgh, 1994), p. 43.
[23] G. C. Stutzin, R. M. Ostrom, A. Gallagher, and D. M. Tanenbaum, J. Appl. Phys. **74**, 91 (1993).
[24] R. M. Ostrom, D. M. Tanenbaum, and A. Gallagher, Appl. Phys. Lett. **61**, 925 (1992).
[25] D. M. Tanenbaum, Ph.D. thesis, University of Colorado, 1995.
[26] M. A. Lampert and P. Mark, *Current Injection in Solids* (Academic, New York, 1970).
[27] M. Wraback and J. Tauc, Phys. Rev. Lett. **69**, 3682 (1992).
[28] A. Gallagher, in *Plasma Synthesis and Etching of Electronic Materials* (Ref. 4), p. 99.
[29] F. Family and T. Vicsek, J. Phys. A **18**, L75 (1985).
[30] R. Bruinsma, R. P. U. Karunasiri, and J. Rudnick, in *NATO Advanced Research Workshop on Kinetics of Ordering and Growth Surfaces*, edited by M. G. Lagally (Plenum, Acquafredda di Maratea, 1989), p. 395.

[31] P. Meakin, Phys. Rep. **235**, 189 (1993).
[32] M. Kardar, G. Parisi, and Y. Zhang, Phys. Rev. Lett. **56**, 889 (1986).
[33] Z. Zhang, J. Detch, and H. Metiu, Phys. Rev. B **48**, 4972 (1993).
[34] A. M. Antoine and B. Drévillon, J. Appl. Phys. **63**, 360 (1988).
[35] A. Canillas, E. Bertran, J. L. Andújar, and B. Drévillon, J. Appl. Phys. **68**, 2752 (1990).
[36] I. An, Y. M. Li, C. R. Wronski, and R. W. Collins, in *Amorphous Silicon Technology—1993*, edited by E. A. Schiff *et al.*, MRS Symposia Proceedings No. 297 (Materials Research Society, Pittsburgh, 1993), p. 43.
[37] R. W. Collins and J. M. Cavese, J. Appl. Phys. **60**, 4169 (1986).
[38] R. W. Collins and B. Y. Yang, J. Vac. Sci. Technol. B **7**, 1155 (1989).
[39] J. Koh, Y. Lu, S. Kim, J. S. Burnham, C. R. Wronski, and R. W. Collins, Appl. Phys. Lett. **67**, 2669 (1995).
[40] Y. Lu, S. Kim, J. S. Burnham, I.-S. Chen, Y. Lee, Y. E. Strausser, C. R. Wronski, and R. W. Collins, in *Amorphous Silicon Technology—1995*, edited by M. Hack *et al.*, MRS Symposia Proceedings No. 377 (Materials Research Society, Pittsburgh, 1995), p. 603.
[41] L. L. Kazmerski (unpublished).
[42] R. Wiesendanger, L. Rósenthaler, H. R. Hidber, H.-J. Güntherodt, A. W. McKinnon, and W. E. Spear, J. Appl. Phys. **63**, 4515 (1988).
[43] J. Jahanmir, P. E. West, S. Hsieh, and T. N. Rhodin, J. Appl. Phys. **65**, 2064 (1989).
[44] E. Hartmann, R. J. Behm, G. Krötz, G. Müller, and F. Koch, Appl. Phys. Lett. **59**, 2136 (1991).
[45] J. J. Boland and G. N. Parsons, Science **256**, 1304 (1992).
[46] K. Ikuta, K. Tanaka, S. Yamasaki, K. Miki, and A. Matsuda, Appl. Phys. Lett. **65**, 1760 (1994).
[47] K. Ikuta, Y. Toyoshima, S. Yamasaki, A. Matsuda, and K. Tanaka, Jpn. J. Appl. Phys. Part 2 **34**, 2379 (1995).
[48] G. J. Vandentop, P. A. P. Nascente, M. Kawasaki, D. F. Ogletree, G. A. Somorjai, and M. Salmeron, J. Vac. Sci. Technol. A **9**, 2273 (1991).
[49] H. Deki, M. Fukuda, S. Miyazaki, and M. Hirose (unpublished).
[50] G. Ganguly and A. Matusda, Phys. Rev. B **47**, 3661 (1993).
[51] W. M. Tong, E. J. Snyder, R. S. Williams, A. Yanase, Y. Segawa, and M. S. Anderson, Surf. Sci. Lett. **277**, L63 (1992).